Localized corrosion attack on the galvanised steel pipes of the fire protection system

Košťúr R.[1], *Kouřil M.*[2]
[1] **Institute of Inorganic Technologies and Materials, Slovak University of Technology, Radlinského 9, 812 37 Bratislava, Slovakia.**
[2] **Department of Metals and Corrosion Engineering, University of Chemistry and Technology Prague, Technická 5, 166 28 Praha 6 – Dejvice, Czech Republic**
E-mail: roman.kostur@stuba.sk

Galvanised steel serves as a base material for pipelines in fire protection systems. However, this system is known for its occasional corrosion failures. The Systems with residual water and oxygen access contribute to formation of macrocells due to different aeration, which can lead to severe damage of the pipes. The aim of this work was to investigate the cause of localized corrosion on the galvanised pipes designated for the fire protection system. The results proved that the main cause of the fire protection pipe system was the residual water in the pipe. The influence of differential aeration on the corrosion of zinc and steel was studied by resistometric technique and showed no effect on the failure of material.

INTRODUCTION

In general, the fire protection system (FPS) includes wet, dry systems, and protection systems. Corrosion attack and the resulting corrosion products can significantly limit the flow of water to the sprinklers and mechanically damage the FPS equipment. Corrosion of the pipes and water leakage are caused by several factors or their combinations including pipe weld corrosion, residual water in dry pipe systems, trapped air in wet pipe systems, water corrosivity, periodic supply of oxygenated water to the system, standing water and microbiologically influenced corrosion (MIC) etc [1, 2]. Identification of the corrosion cause on galvanised pipes becomes a difficult task due to possible combination of the above-mentioned factors [3],[4].

Pipe material

In addition, the pipe material also influences the extent and course of pipe corrosion in FPS. Currently, according to NFPA (National Fire Protection Association) standards, especially the NFPA 13 [5], it is allowed to use metallic and non-metallic materials for FPS pipes that meet the ASTM (American Society for Testing and Materials) requirements. Most often, the standard accepts copper, iron-based, and plastic pipes. The iron-based pipes are dividing into stainless steel or galvanised steel. The main advantage of using plastic pipes, as opposed to metal ones, is their low susceptibility to corrosion. However, this fact is balanced by a limited range of acceptable temperatures, dominated by metal pipes with a melting point above 1400 °C (for Fe) and 1000 °C (for Cu) [6]. The advantages of using polypropylene pipe (PP) include long service life (up to 50 years), easy assembly and handling, environmental friendliness, and recyclability. However, it can withstand temperatures up to 90 °C and for a limited time up to 110 °C, so it is predisposed to use in 'light danger' [7]. The disadvantage of galvanised steel is that it is more susceptible to corrosion than any other FPS piping material. Occasionally, corrosion failures occur shortly after installation [8].

Corrosion

In the case of galvanised steel pipes, both the internal and external surfaces of the pipe are covered with a zinc coating. When the zinc layer on the surface is perforated, zinc in relation to the steel substrate behaves as a sacrificial anode in a corrosive environment. It preferentially corrodes ($Zn = Zn^{2+} + 2e^-$), thus electrochemically protecting this steel substrate [9]. This protection consists in the formation of alkaline salts, primarily carbonates, which represent a barrier against corrosion. The most common phase is hydrozincite – $Zn_5(OH)_6(CO_3)_2$.

In places where the zinc coating is damaged, local corrosion occurs and exposes the steel substrate, which remains cathodically protected [10]. If there is further dissolution of the zinc coating in this place, the exposed steel base widens, and the protective function of the zinc is no longer sufficient. The exposed steel begins to corrode locally ($Fe = Fe^{2+} + 2e^-$), forming "tubercules" (Fig. 1). The formation of this complex structure can be conditioned by microbiological activity [11] or abiotic factors. The chemical composition of tubercules is complex, it differs in different places of the tubercule, and it is conditioned by its complex structure.

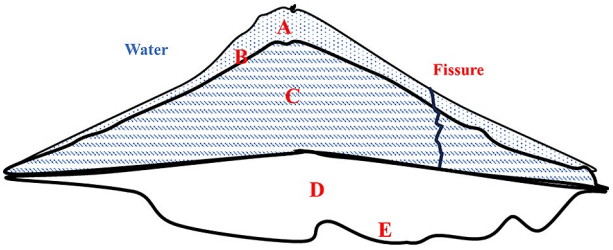

Fig. 1. Complex structure of tubercule without MIC corrosion [2] – A) outer crust, B) inner shell, C) core material, D) fluid-filled cavity, and E) corroded floor

Pitting corrosion – "pitting" is one of the most common types of corrosion encountered by FPS pipes. It is characterized by highly localized metal loss, and it appears as a deep, small hole in an otherwise intact surface [10]. Because "pitting" often occurs under corrosion products, such as tubercules, identification of this type of corrosion tends to be difficult [12]. A problem is the complete perforation of the pipe [13], so that liquid could leaks from the pipe. The shielding of the surface by corrosion products leads to the limitation of oxygen transfer to the metal surface, which can cause local acceleration of corrosion due to the action of the differential aeration cell.

Another problem that can cause damage to FPS pipes is weld/seam corrosion. This special type of corrosion can be attributed to the formation of unstable iron sulphides together with high residual stresses and microstructural changes around the weld seam areas. This causes the formation of anodic spots where corrosion can occur [2]. Such places can already be created during factory production and include the weld seam and heat-affected zones.

Weld corrosion and pitting are promoted by reduction of dissolved oxygen. Both pitting and weld corrosion aggressively consume metal from the pipe wall. However, the result is different. Weld corrosion creates a narrow groove on the weld surface along the length of the pipe [14].

Precautions

There are several options to prevent or slow down the corrosion of FPS pipes. If the dominant factor causing the corrosion of the internal surface of the pipe is the residual water in the pipe, then the precautions could be the following.

Correct inclination of pipes for water drainage is essential. This should be focused on when installing the FPS system. If it is possible to remove all the water from the system (an unrealistic ideal), care must be taken to ensure that the supplied air is as dry as possible. The application of air dryers is recommended. Alternatively, nitrogen can be used to limit the access of oxygen to the system, eventually pressurising the system completely, with only nitrogen. However, this precaution is economically disadvantageous [2,15].

Problem specification

The main goal of this work is to specify the cause of the local corrosion attack on the pipes of a fire protection system and to discuss reasonable corrosion protection countermeasures.

The fire protection system was flooded with water for the first time during a distribution system pressure test at an operating pressure of 9 bar in July 2018. The water used for the extinguishing system is tap water without previous treatment as it is usual. The next flooding, approx. 3 times since the time of implementation, occurred in the event of a malfunction/accidental start-up of the FPS system. The distribution was subsequently drained through the sludge removal system and repressurized. During the next three days, the water was gradually released under pressure through the sewage systems on each floor. Since then, the dry distribution has been permanently pressurized to 3 bars. Regular system tests (flooding) are not normally performed. The system was flooded only once during building approval. However, several pipe perforations occurred within 3 years. The customer wanted to remain anonymous and did not provide further information.

EXPERIMENTAL

Description of galvanised steel pipes

Galvanised pipeline samples were taken from the damaged parts of the FPS. The material of the samples was hot-dip galvanised steel. The inner diameter of the pipe was 82 mm, the outer diameter of the pipe was 89 mm. A visual evaluation of the damage that occurred on the outer and inner parts was carried out. For further

Fig. 2. Representation of the clock system at the pipe from FPS

description, a system of identifying the position along the horizontal pipe circumference corresponding to the clock was introduced (Fig. 2). The sixth o'clock corresponds to the position of the lowest place in the pipe. The symmetric distribution of deposits and corrosion products on the inner surface confirms the validity of this approach and reveals long-term partial flooding of the pipe with water.

The external surface of the pipe (Fig. 3) did not show any serious signs of damage, except for the perforation (Fig. 3b). In certain places, it is possible to observe a rough structure on the surface – „semolina" (Fig. 3a), which arises when the equilibrium conditions change during the galvanizing process.

The internal surface of the pipeline before sampling is shown in Figure 4a. The internal surface is covered with white particles of zinc corrosion products. It is more intensively visible in the lower part of the pipe, from about 4 o'clock to 8 o'clock. This corresponds to a probable water level in the pipeline, which is estimated to be 40%. A row of three tubercules is observed at 5 o'clock. A few small tubercule germs also appear in position 2 o'clock, indicating that the level stopped for some time at this place as well. In addition to the white corrosion products of Zn, the orange corrosion products on the internal surface (iron corrosion products) can be found. At approximately 10 o'clock to 2 o'clock positions, corrosion products are scattered unevenly over the surface. It is assumed that this area (10-2 o'clock) was not exposed to standing water. The direction of water flow in the pipeline is observed on the deposits of corrosion products.

A macroscopic detail of one tubercule is shown in Figure 4b. The colour of the tubercule is orange-brown, and from one side, a cavity of the tubercule and its layering can be seen. The area around the tubercule is surrounded by a solid layer of white corrosion products. There are also orange spots and black dots.

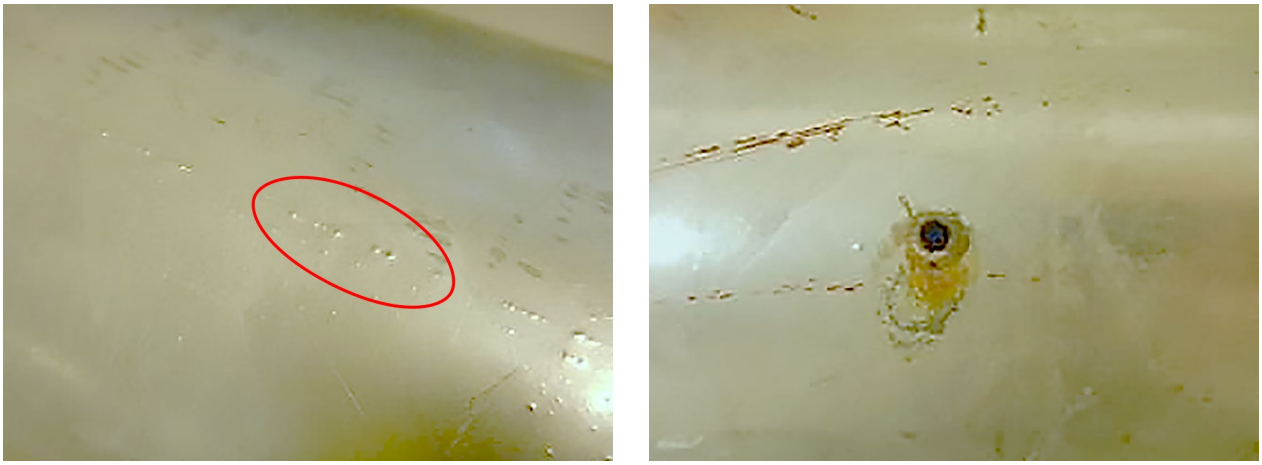

a) b)

Fig. 3. Photo documentation of the outer surface of the pipe

a) b)

Fig. 4. The internal surface of the sample with macroscopic detail of one of the tubercules

Samples preparation

Powder samples

The powder samples of the tubercule and the bottom powder samples were taken from the internal surface of the pipe in the area where the water level was expected to occur. The top powder sample was taken from an internal surface of the pipe in the place outside the assumed water level.

To identify corrosion products on the internal surface, a sample (2 × 2 cm) with a tubercule was cut from the pipe. This tubercule was then crushed to a fine powder – "tubercule powder sample". A white and orange layer of corrosion products was scraped from the lower part of the pipe (approx. 4-6 o'clock) – "bottom powder sample", and a white layer of corrosion products was scraped from the upper part (10-12 o'clock) "top powder sample".

Whole samples

Samples were taken from the pipe marked with coloured rectangles in Figure 5. The taken samples, cross-sections, served as the basis for further analyses. The cross-section samples were embedded into a two-component epoxy, so that the adhesion of the corrosion products and the metal was ensured, thereby preserving the structure of the corrosion products. Subsequently, the metallographic cut prepared in this way was ground using SiC grinding paper with various grain sizes (P80 – P2500) under running water, polished without water with diamond paste D2, rinsed with ethanol, and dried with a hot air fan.

EDX analysis

Elemental composition analysis using energy dispersive analysis (EDX) was performed on 2 types of samples:

a) powder samples (3×),
- bottom; top; tubercule,

b) analysis on "cross-sections" samples,
- tubercule (Fig. 5 blue rectangle),
- place after ridding of the tubercule (Fig. 5 yellow rectangle).

Electron scanning microscope (Tescan Vega 3 40HV, Czech Republic) with EDS analyzer Oxford X-max (Great Britain) was used.

XRD analysis

The identification of the crystalline phases was carried out using X-ray diffraction analysis of the 3 powder samples:

- bottom
- top
- tubercule

Powder XRD data were measured at room temperature on an X'Pert PRO θ-θ powder diffractometer in Bragg-Brentano parafocusing geometry using Co-Kα wavelength (λ = 1.7890 Å, U = 35 k). Data were unscanned using an ultrafast 1D detector X'Celerator in the angular range of 5-60° (2θ) with a measurement step of 0.039° (2θ) and a reading time of 15.21 s step-1 Data evaluation was performed with the program HighScore Plus 4.0.

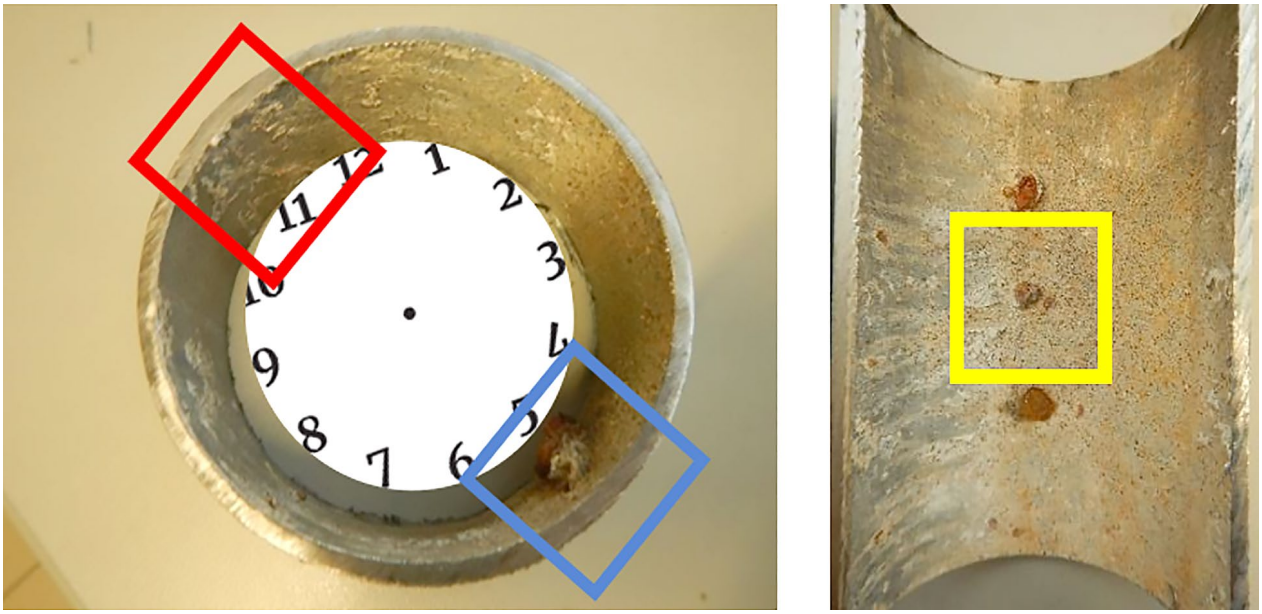

Fig. 5. Sections of the pipeline with marked sampling areas for the preparation of metallographic samples

Optical microscopy

The quality of galvanization and the structure of the steel substrate was evaluated using metallographic samples. The Nikon Eclipse MA200 optical microscope at various magnifications was used to observe three samples (Fig. 5). For each sample, the zinc layer on the internal and external parts was evaluated. Before evaluation, the samples were etched with Nital (1% solution), except sample with the tubercule.

Resistometric measurements

To analyse the corrosion behaviour of zinc in aerated conditions, resistometric measurements were performed. The experiment was conducted on 2 types of the AirCorr resistometric sensors: Zn 50 µm and Fe 25 µm (Fig. 6a). Schematic picture of a resistometric sensor is on the Figure 6b). The principle of the resistometric method as a corrosion monitoring consists in measuring the electrical resistance. When the metal corrodes, the thickness of the metal track is getting lower, and therefore the resistance higher. There are two parts of the sensor – the measuring part and the reference part.

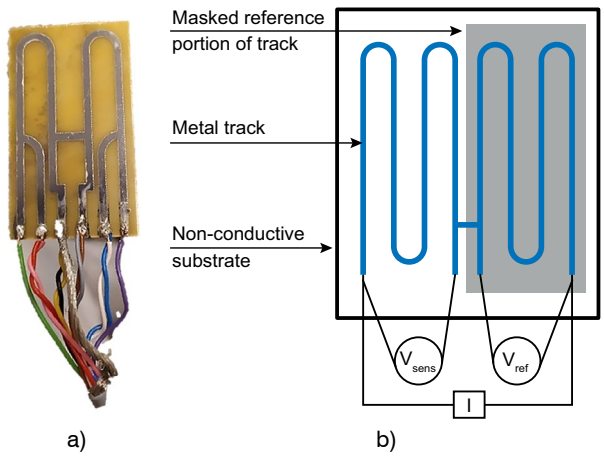

Fig. 6. Display of Aircorr sensors: a) real Fe 25 μm AirCorr resistometric sensor, b) schematic image of the resistometric sensor [16]

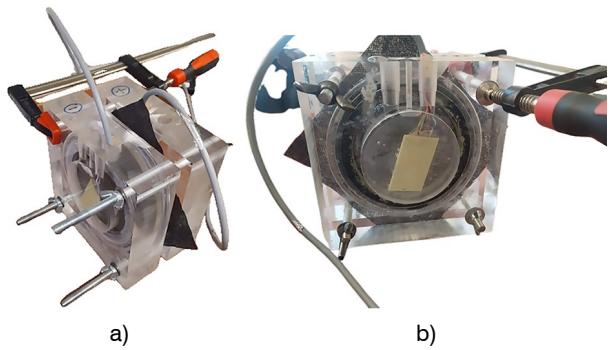

Fig. 7. PMMA cell with connected resistometric sensors

The measuring part is in contact with the environment, and the reference part is masked and is not in the contact with the environment, the main role of the reference part is to compensate the temperatures changes. This method provides real-time monitoring of the corrosion depth [16,17].

The prepared samples were stored in PMMA cells, where two sensors were always facing each other.

The space of the two sensors was separated by a permeable fabric and insulated with rubber gaskets. A cell prepared in this way can be seen in Figure 7.

The cell was filled with tap water and the individual sensors were connected to the Zahner X electrochemical workstation. First of the sensors was connected as a working electrode and the other one as a counter electrode, with the assumption that the first would act as an anode in the thus created galvanic cell. The working electrode was then potentiostatically polarized to 0 mV with respect to the counter electrode. Thus, the potential difference between the zinc and steel sensors was zero, and the recorded current corresponded to the macrocell current. At the same time, resistometric sensors recorded the corrosion loss of both metals in the cell.

In the resistometric experiment, 4 different combinations of cells were chosen:

- Zinc in oxygenated water versus zinc in deoxygenated water;
- Zinc in oxygenated water versus steel in deoxygenated water;
- Zinc in deoxygenated water versus steel in deoxygenated water;
- Steel in deoxygenated water versus steel in oxygenated water.

The measurement was performed for 24 hours without purging with a gas and for 24 hours with purging with the appropriate gas. At the same time, the change in the thickness of the measuring part of the sensor was reported.

RESULTS

EDX results

All results from EDX analysis are summarized in Tables 1-3.

Powder samples

The powder samples were obtained from the internal part of the pipe. It's clearly seen from the results (Tab. 1) that the samples from the top and bottom part of the pipeline are mainly composed of corrosion products of zinc. They also contain trace amounts of elements (Ca, Si, Na, and others) probably originating from water. The top part means the area outside of the assumed

Tab. 1 Elemental composition of EDX analysis of pipeline samples for powder samples of corrosion products (at. %)

Measurement area	Fe	Zn	C	O	Ca	Si	Na	S	Cl	others
top I	0.2	12.5	49.5	30.7	0.3	0	6.8	0	0	–
top II	0.6	25	29.1	37.8	0.4	0.1	6.8	0	0	0.2
bottom I	0.7	25.3	25.1	41.1	0.2	0.2	6.7	0	0	0.7
bottom II	0.4	21.1	21.4	45.8	0.2	0.3	10.1	0	0	0.7
tubercule	11.5	1.3	44.8	42.1	0	0	–	0	0	0.3
tubercule II	20.9	2.3	16.1	60.4	0	0.1	–	0.1	0	0.1

water level, while the bottom part means the area of the assumed water level.

The analysis of the crushed tubercule (Tab. 1 tubercule) points to the fact that it was formed mainly by corrosion products of iron. These analyses also aimed at detecting the presence of chlorides and sulphur, which were not detected. The presence of C and O was confirmed, but the values given in the tables are only indicative.

Cross-section- place after ridding of the tubercule

From the cross-section analysis of the sample with an empty space up to the tubercule, the internal surface (below the water level) was analysed, on which there was a flooded place up to the tubercules at about 4.5 o'clock. On the right side, along the internal circumference from the tubercule, there is a "leap" (on the dial at about 3.5-4 o'clock), which is probably related to the weld.

Tab. 2 Elemental composition of EDX analysis of pipe samples for the internal surface of the cross-section sample with weld (at. %/wt.%)

Measurement area	Fe	Zn	C	O	Na	type
1	7.4	92.6	–	–	–	wt.%
2	1.4	34.5	21.8	32.3	9.9	at. %
3	0.5	26.9	17.6	46.4	8.7	at. %
4	–	70.2	29.8	–	–	at. %

The results are summarized in Table 2, where the measurement areas are differentiated according to the position of the assumed weld. The relevant measurement areas are shown in Figure 8, while the following conclusions were made:

- measurement area 1 is formed by an intermetallic phase of Fe and Zn (probably δ phase – 7-11 % Fe),
- areas marked as 2-3 are formed by corrosion products of Zn (a prerequisite for more complex compounds such as carbonates, bicarbonates, etc.),
- area 4 represents the rest of the η phase, pure Zn.

Cross-section - with the position of the tubercule

The results of the analysis on the internal surface of the cross-section sample with the entire tubercule are summarized in Tab. 3 and the measurement areas are shown in Fig. 9.

This is a sample whose entire internal surface was below the water level with the tubercule in the position at 5 o'clock. From the measured values, it can be concluded:

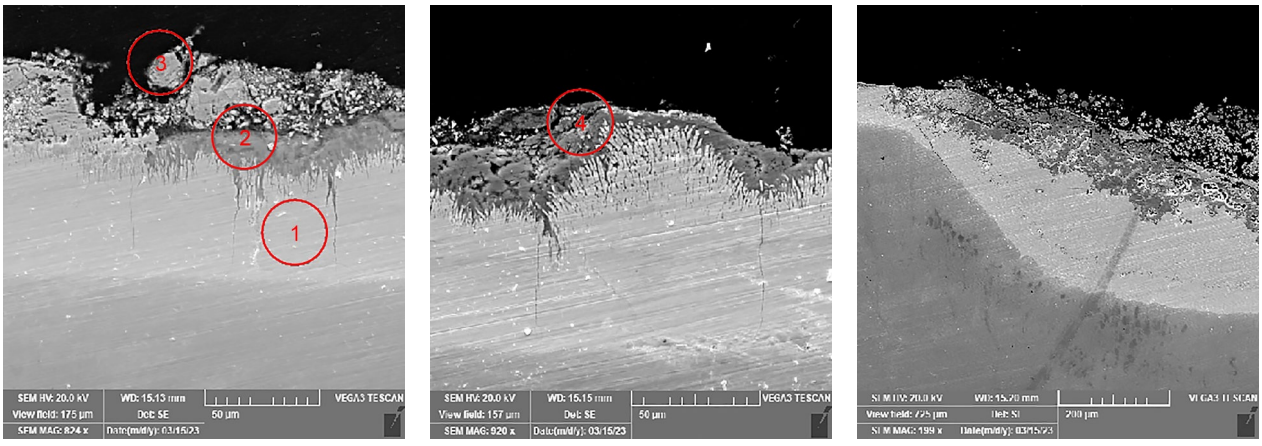

a) b) c)

Fig. 8. SEM images from a cross-section measurement of a welded sample with marked measurement areas a) left from the leap, b) right from the leap, c) the leap

- two areas (1 and 2) of the outer part of the tubercule are formed mainly by corrosion products of Zn (the resulting tubercule probably took with it the corrosion products that formed on the internal surface of the pipe),
- areas 3-5 marked in Figure 9 are formed by Fe corrosion products,
- the presence of chlorine and sulphur was detected inside the tubercule (up to 1 wt.%), in the case of the external layer of the tubercule it was not detected,
- the pipeline wall is weakened due to the occurrence of tubercules and corrosion attack.

RTG analysis

The results of X-ray diffraction analysis revealed the presence of the following crystalline phases (Tab. 4) on individual powder samples. Semi-quantitative analysis at Table 5 determined the approximate composition of individual powders.

Tab. 4 Legend of crystalline phase

G – goethite	**H – hematite**
W – wulfingite	**L – lepidocrocite**
Z – zincite	**HZ – hydrozincite**
M – magnetite	**C – calcite**

The tubercule is formed mainly by corrosion products of Fe – goethite, hematite, magnetite (anaerobic conditions inside the tubercule) and lepidocrocite. Tubercule powder also contains trace amounts of akagenite (β -FeO(OH)), which isn't displayed on Tab. 5. This confirms the contribution of chlorides in the corrosion mechanism. Both the top and the bottom powder samples are formed by corrosion products of Zn – zincite, wulfingite, and hydrozincite. Calcite, originating from hard water, was also identified here.

Tab. 3 Elemental composition of EDX analysis of pipe samples for cross-section sample with whole tubercule (wt.%)

Measurement area	Fe	Zn	C	O	Na	Ca	Al	S	Cl	others
1	15.8	36.6	15.7	26.1	5.4	0.3	-	–	0.1	–
2	30.1	29.8	10.5	25.2	4.1	0.2	0.1	–	–	–
3	31.5	0.6	47.6	17.1	–	0.4	0.4	0.6	0.4	1.4
4	58.4	0.6	14.9	23.4	–	0.3	0.5	0.5	0.1	1.3
5	24.3	0.8	55.6	18.2	–	–	–	0.3	0.8	–

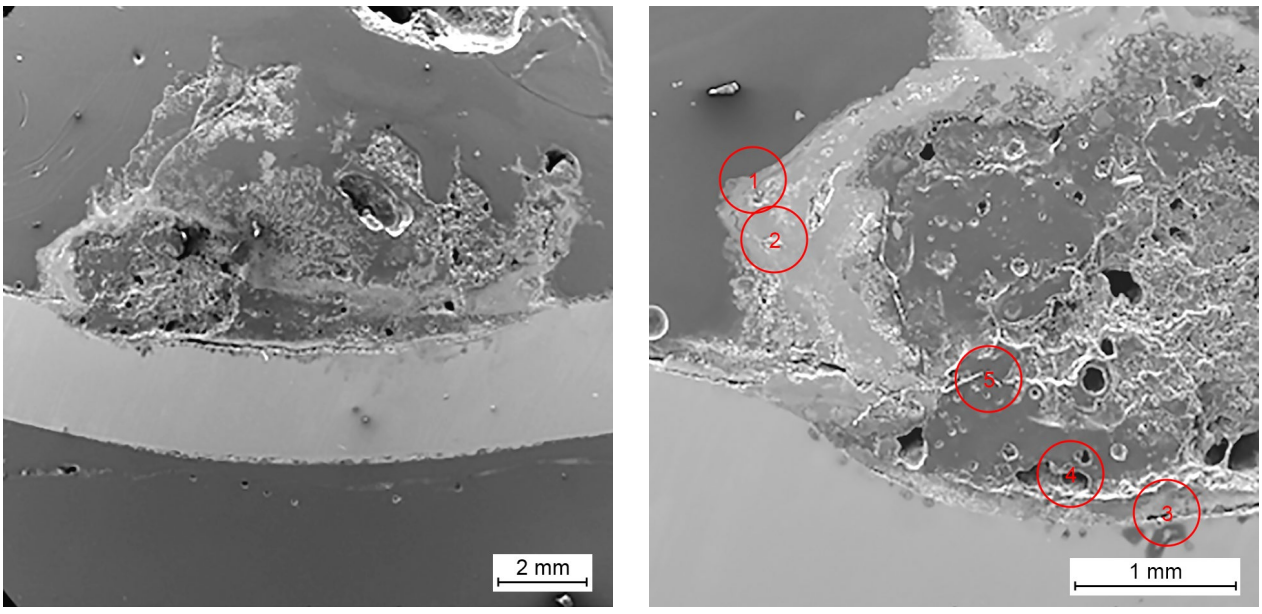

a) b)

Fig. 9. SEM images from the cross-section analysis of the sample with marked measurement areas

Tab. 5 Semiquantitative analysis for individual powder samples

	G α-FeO(OH)	**H** Fe_2O_3	**Z** ZnO	**HZ** $Zn_5(CO_3)_2(OH)_6$	**W** $Zn(OH)_2$	**L** γ -FeO(OH)	**M** Fe_3O_4	**C** $CaCO_3$
Tubercule	~50%	~20%	~2%	traces	–	~18%	~10%	–
Top	traces	traces	~75%	~15%	~5%	–	–	~5%
Bottom	–	traces	~75%	~5%	~15%	–	–	~5%

Optical microscopy

The optical microscopy results were aimed at assessing the condition of the zinc coating and the underlying steel in relation to the assumed conditions of exposure on the inside and the assumed presence of the weld.

Identification of the type of steel and the state of galvanization was carried out after etching the sample. The microstructure of the steel is shown in Figure 10. This is the microstructure of the base material outside the damage area. This steel corresponds to a ferritic-pearlitic structure with a low carbon content [18].

In Figure 11, the microstructure of the underlying steel is observed, focusing on the search for the weld, that was identified. This weld is located, as expected, on the lower part of the pipe (approximately at 3.5-4 o'clock).

The microstructure of the zinc coating with individual phases for the outer part of the sample out of the damage area is shown in Figure 12. It is possible to recognize all relevant Fe-Zn phases up to the pure *η*-phase of Zn. This image is considered as a reference for determining the Fe-Zn phases for other etched samples.

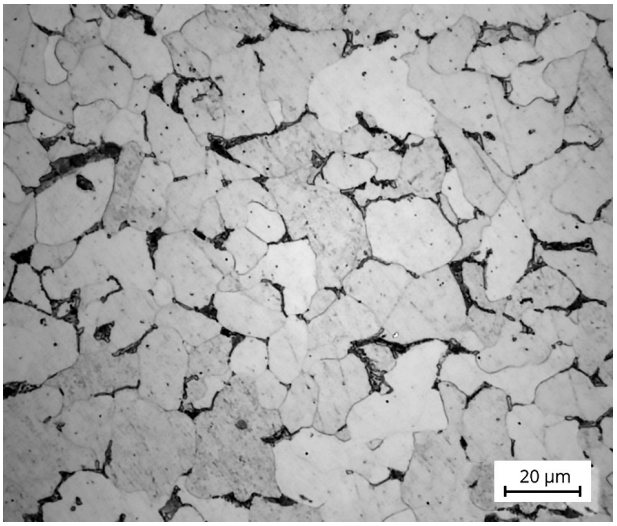

Fig. 10. Microstructure of steel sample after etching (Nital 1%)

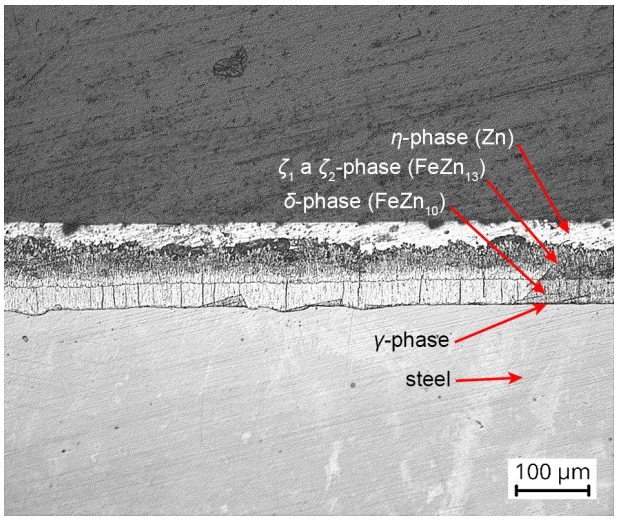

Fig. 12. Zinc coating microstructure at the external part of the sample after etching (Nital 1%)

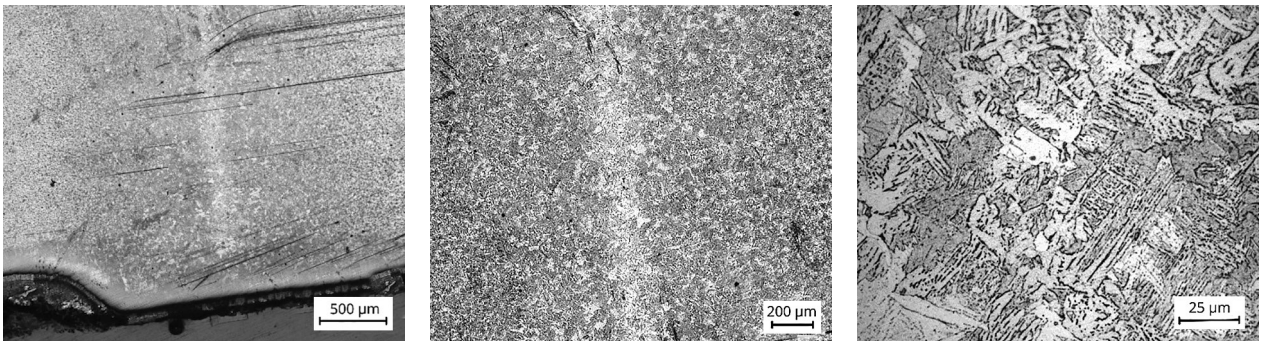

a) b) c)

Fig. 11. Microstructure of the steel sample with detail on the weld

The area out of the assumed water level (10-12 o'clock)

The evaluation of the zinc coating with individual phases for the internal/external part of the sample from the area out of the assumed water level is shown in Figure 13. The condition of the external part (Fig. 13c,d) does not show any significant damage. In Fig. 13c, an unevenness in the zinc layer is captured, but it is assumed that this is only mechanical damage. The overall condition of the internal part of the zinc coating shows visible damage even at the smallest magnification. In certain places of the surface, it is possible to observe voids, which were probably created due to pitting corrosion (Fig. 13a,b).

It is possible to distinguish all relevant phases of the zinc coating up to the pure η-phase of Zn (Fig. 14a,b) for both parts of the sample. The damage of internal part of the sample can also be confirmed due to the microstructure of the zinc coating (Fig. 14b). The underlying ζ-phase remains intact. The residual thickness of the zinc coating at the damage sites therefore remains 80 to 90 µm.

The area of the assumed water level (4-6 o'clock)

The evaluation of the zinc coating with individual phases for the internal/external part of the sample from the area of the assumed water level is shown in Figures 15-16. The internal part of the sample containing the entire tubercule is observed in Figures 15a,b, and 16a,b. The damage penetrates to the steel substrate itself, in some places the zinc coating is not present at all (Fig. 16a). Elsewhere, lower layers of the coating persist – mainly intermetallic phases (ζ_1 and ζ_2-phases, δ-phase). The overall view of the external part of the sample with the tubercule is shown in Figures 15c and 16c. The condition of the external part shows less damage, along the zinc layer, but it's mostly well preserved.

When comparing the overall damage to the pipeline at two different locations (out of the assumed water level/ at the assumed water level), the following conclusions can be drawn:

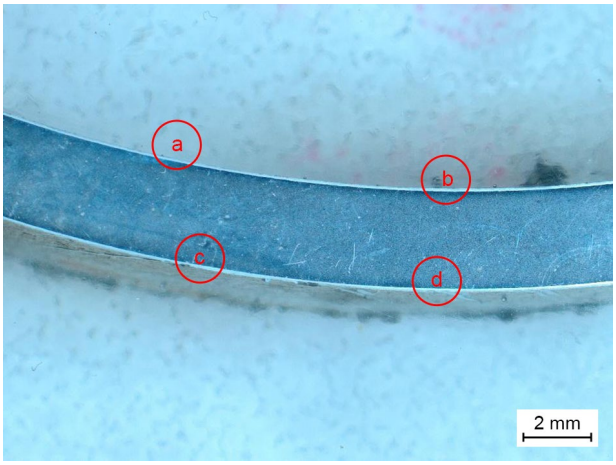

a)

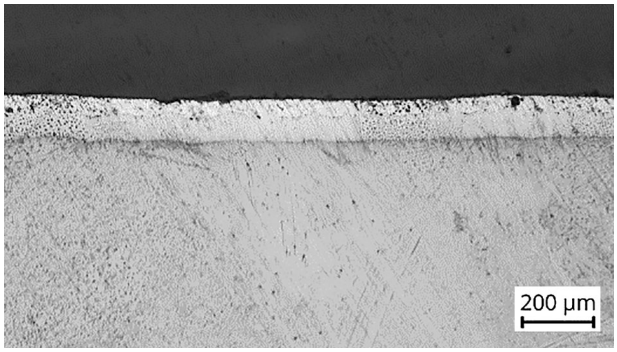

b)

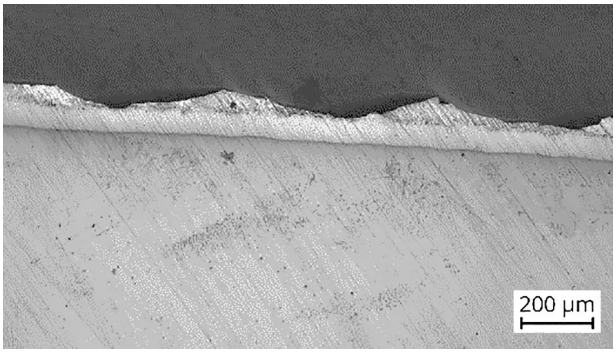

c)

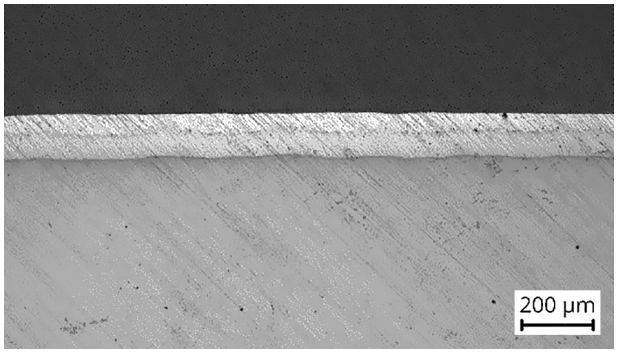

d)

Fig. 13. The state of the zinc coating of the surface of sample outside the assumed water level-overall view and marked areas observed using an optical microscope

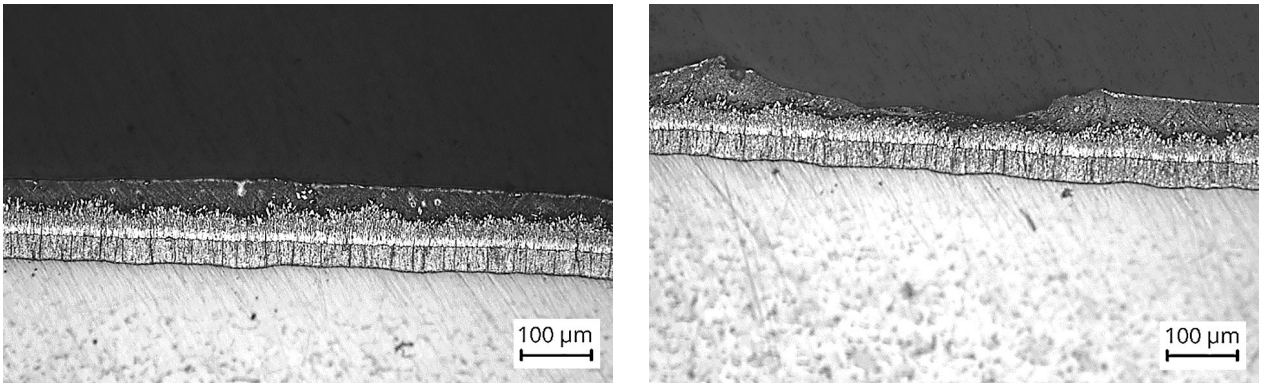

a)

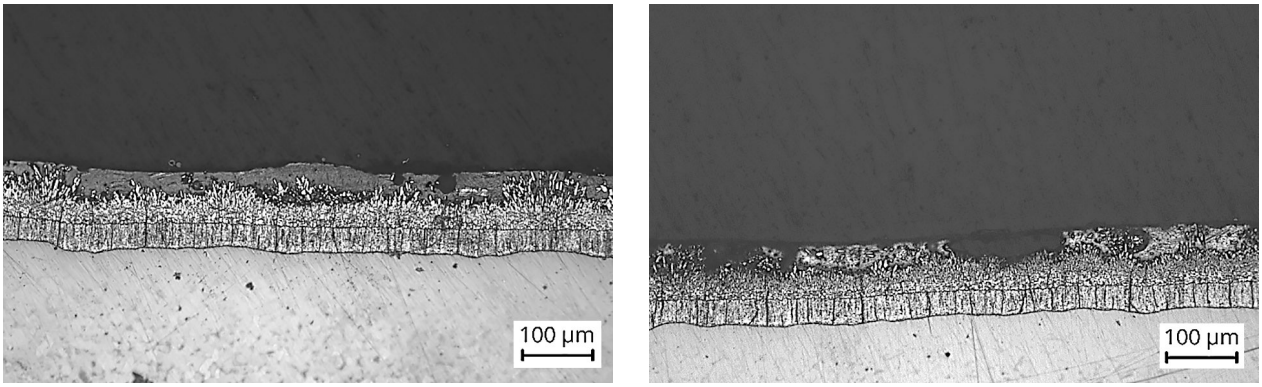

b)

Fig. 14. The microstructure of the zinc coating of the external (a) and internal (b) surface of the sample, outside the assumed water level, after etching with identified damages on the surface

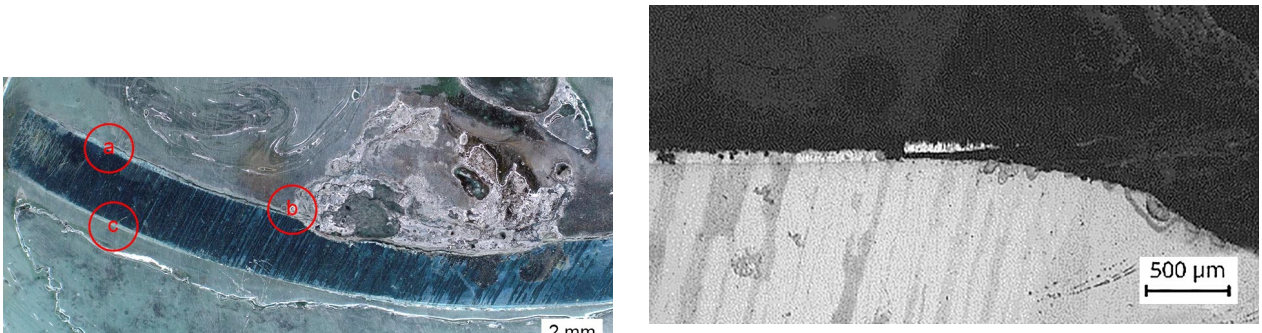

b)

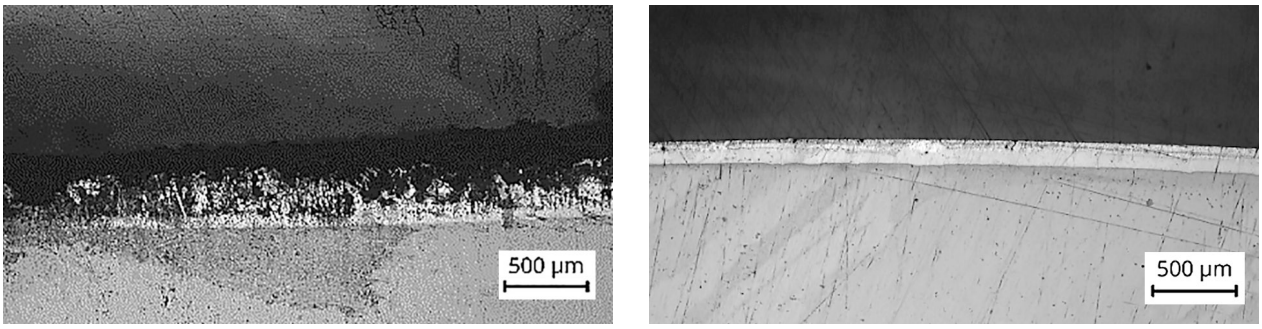

a) c)

Fig. 15. Overall view of the zinc coating of the external/internal surface of the pipe sample with tubercule-marked areas observed using an optical microscope

- damage to the internal surface is greater compared to damage to the external surface within the comparison of each sample separately,
- damage to the internal and external surfaces is greater in the sample that contained a tubercule (at the assumed water level),
- the state of the zinc coating outside the area of the tubercule (outside the assumed water level) is satisfactory, the galvanization layer (external and internal) still provides a certain corrosion resistance,
- the condition of the zinc coating inside the tubercule sample is not satisfactory, the zinc coating on the internal surface does not provide corrosion protection, corrosion attacks the steel substrate; damage can be seen in the coating on the external surface, but this layer still provides some protection against corrosion.

Evaluation of the coating thickness

In each sample, the thickness of the zinc coating was measured 5 times to get an average value. It was measured by microscopical method. Two measurement locations were chosen, outside of the tubercule, and the second one inside the tubercule. The results of zinc coating thickness were doublechecked and confirmed, shown in Tab. 6. The ext/int marking in the name of the sample refers to the external or internal surface of the sample. The table shows the average thickness value d with its standard deviation σ.

From these results, the sample outside the tubercule area (10-12 hours), which had the least damaged zinc layer, has both parts of the sample (external and internal) with approximately the same thickness (115 µm). On the contrary, the sample on the same pipe, which is located at 4-6 o'clock, with a tubercule, showed great damage of the zinc layer, mainly inside the tubercule. This was also confirmed in the optical microscope images (Figs. 15a,b and 16a,b). When measuring the thickness of the zinc layer, the focus was only on the zinc coating that remained on the edge of the tubercule. The maximum values of the layer thickness here reached approximately 65 µm. The thickness value for the external layer, measured outside the „damage", reached 126-133 µm. It's believed that unusual thickness is not an issue in terms of the localized corrosion.

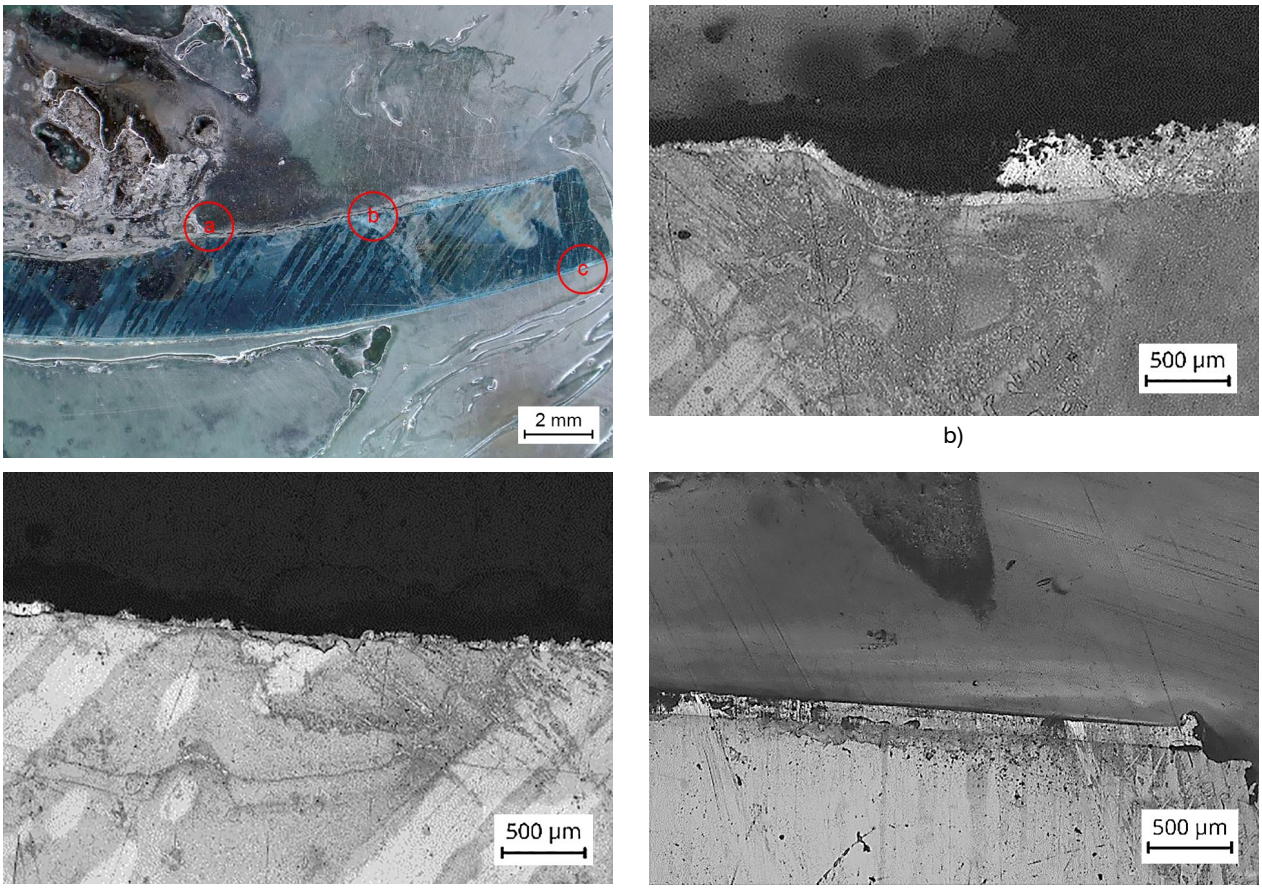

a) b) c)

Fig. 16. Overall view of the zinc coating of the external/internal surface of the pipe sample with tubercule-marked areas observed using an optical microscope

Tab. 6 Thickness of galvanizing layer for pipeline samples (ext--external side; int-internal side)

Sample	d (µm)	σ (µm)
out of tubercule_ext1	99.8	12.1
out of tubercule_ext2	114.2	7.3
out of tubercule_int1	114.4	3.6
out of tubercule_int2	117.2	5.4
tubercule_ext1	125.6	4.3
tubercule_ext2	133.4	4.4
tubercule_int1	64.4	4.4
tubercule_int2	64.8	5.4

Resistometric measurements

The aim of this measurement was to verify whether a cell with differential aeration in possible combinations can have a significant effect on the acceleration of corrosion.

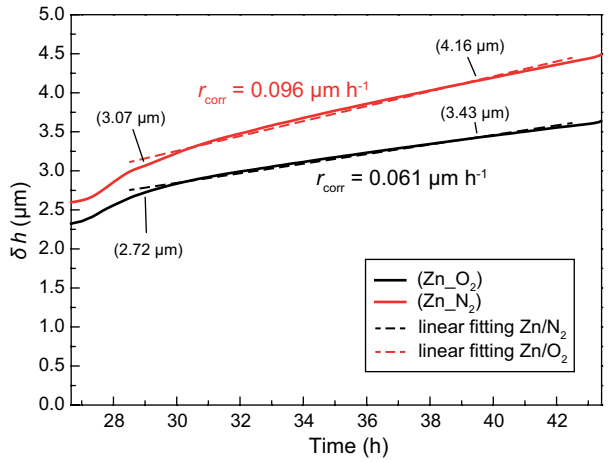

Fig. 17. Comparison of Zn/Fe cells during different aeration with calculated r_{corr} and different δh for the same time during an experiment

The difference between oxygenated zinc (Zn/O_2) and non-oxygenated zinc (Zn/N_2) in connection to macrocell during aeration is shown at Figure 17. Oxygenated zinc does not significantly accelerate the corrosion of non-oxygenated zinc. The corrosion rate – r_{corr} of both increases significantly when the mixing of the electrolyte with the gas is more intense, as shown in the Figure 17. According to the change in sensor thickness – δh, it can be stated, that during the aeration for 24 hours with gases, difference in thickness increased from 0,34 to 0,77 µm. This is a negligible difference. The oxidizing power of the environment is not a dominant factor. As for the change in potentials – E, it is clearly seen from Figure 18, that with aeration, potential of oxygenated zinc shifts into positive values.

The next combination in the experiment consisted of a zinc and steel probe, both exposed to deoxygenated water. The δh record is shown in Figure 19 (Zn/N_2+Fe/

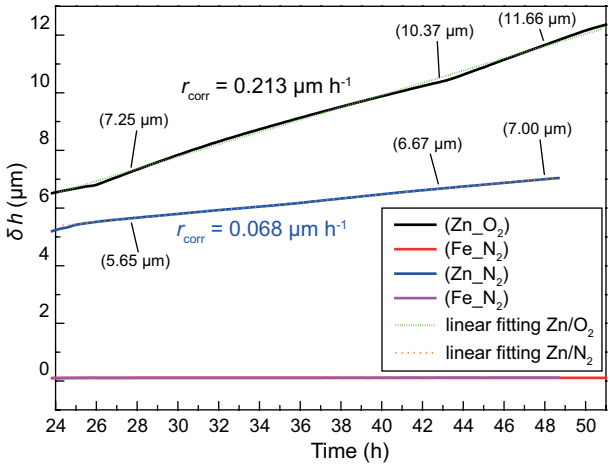

Fig. 19. Comparison of Zn/Fe cells during different aeration with calculated r_{corr} and different δh for the same time during an experiment (first cell – Zn/O_2+Fe/N_2; second cell – Zn/N_2+Fe/N_2)

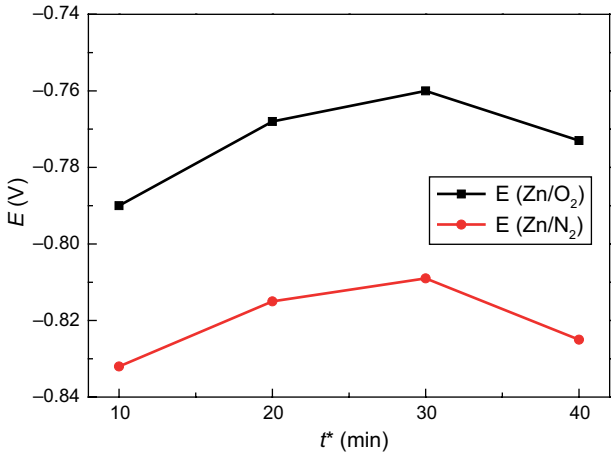

Fig. 18. Potentials of oxidized and non-oxidized zinc in combination Zn/Zn microcell during aeration: E – potential; t^* – time from the start of aeration

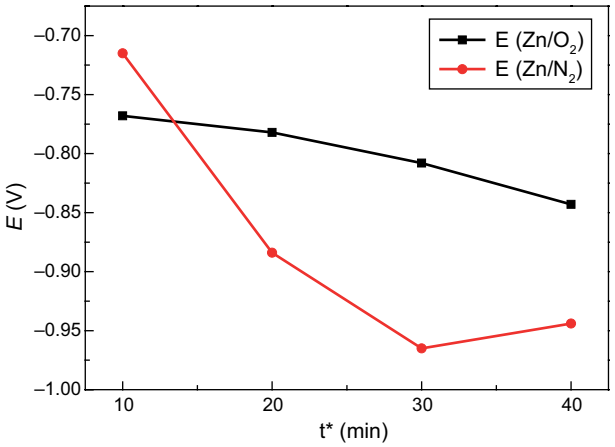

Fig. 20. Potentials of oxidized and non-oxidized zinc in combination with Fe cells during aeration: E – potential; t^* - time from the start of aeration

/N_2). From the comparison with the graph shown in Figure 17, the r_{corr} for zinc in Figure 18 is roughly the same as in the combination of two zinc sensors.

However, zinc corrosion accelerates with O_2 if zinc is combined with steel, which can also be seen at Figure 19 (Zn/O_2+Fe/N_2). Therefore, the potential shifts in the positive direction (Fig. 20), but the corrosion rate is increased by the presence of oxygen.

Acceleration of steel corrosion in a non-oxygenated environment was confirmed at the macrocell Fe/ /N_2+Fe/O_2. Such a combination refers to the connection of an oxygenated and non-oxygenated surface of steel. This is evident from the Figures 21 and 22, as the r_{corr} is higher for the Fe/N_2, and r_{corr} is almost negligible for the Fe/O_2. According to comparison of potentials during aeration, it can be stated that steel in non-oxygenated environment showed higher values of free corrosion potential.

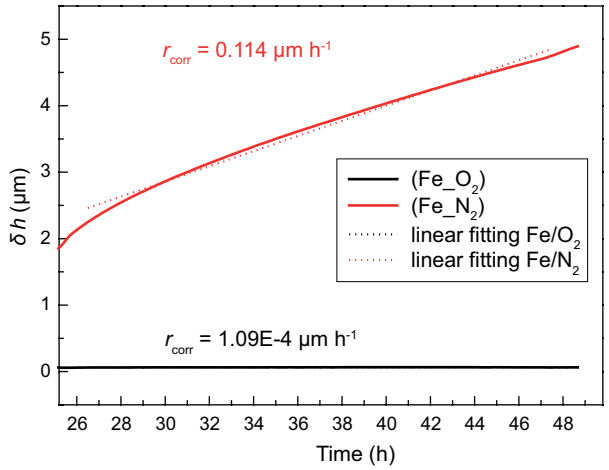

Fig. 21. Comparison of Fe/Fe cell during different aeration with calculated r_{corr} and different δh for the same time during an experiment

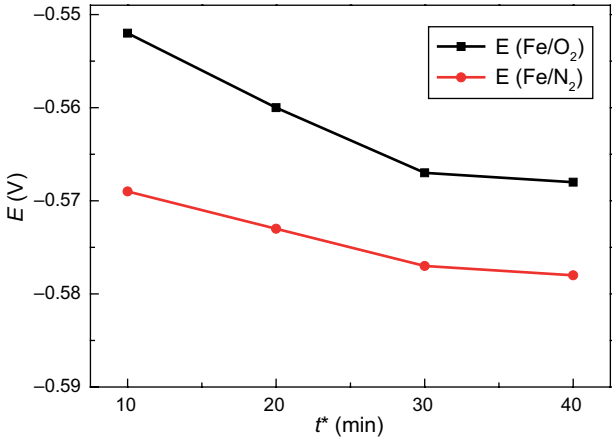

Fig. 22. Potentials of oxidized and non-oxidized steel in combination Fe/Fe cell during aeration: *E* – potential; *t** – time from the start of aeration

DISCUSSION

Galvanised steel is widely used as the basic material in fire protection systems. Zinc provides corrosion protection to carbon steel by corroding more slowly than steel, and by forming zinc corrosion products such as a barrier against iron corrosion.

In „dry pipe“ environments, the main problem is residual water (electrolyte), which accelerates the corrosion process and, in combination with pressurised air inside the pipe resulting in elevated dissolved oxygen and possessing a great risk of extensive corrosion on the internal surface of the pipe, which can lead to perforation through the pipe wall. Due to the concentration gradient of oxygen in the water, a cell with differential aeration is created, firstly in between oxygenated and deoxygenated zinc, later in between oxygenated and deoxygenated steel, which increases the probability of pitting of steel, as well as the growth of tubercules.

This problem was also observed in the pipes that were submitted for the analysis. The corrosion attack was located mainly in the lower part of the pipe (approximately 5 o'clock), where a whole series of tubercules, or their germs, were identified. The appearance of tubercules is related to the position of the water level in the pipe. Since the germs of tubercules are also observed, this is proof that the water level stopped for a certain time in this place as well. In one place of the pipe there was even a perforation that arose under the tubercule. It is also possible to observe how deposits and corrosion products were carried away by water. Since the local corrosion attack is mostly positioned at the residual water layer, the microbiologically influenced corrosion (MIC) is considered to be irrelevant and this factor wasn't studied.

The results of EDX analyses aimed at identifying the elemental composition for several types of samples. These results revealed that the elemental composition of the tubercule (powder sample) does not contain Cl and S (0.1 at. %), it is formed mainly by corrosion products of Fe in various compounds. When this powder sample was analysed by XRD technique, the respective phases goethite, hematite, lepidocrocite, and magnetite (anaerobic conditions inside the tubercule) were identified in the main representation. A small amount of ZnO also appears here as a product of Zn corrosion.

However, analysis of the entire tubercule, from which a metallographic sample was made, proves the presence of Cl and S in the lowest layers of the tubercule (up to 1 wt.%). This can also be seen on the EDX cross-section analysis of this sample.

EDX analyses for powder samples from the lower part of the pipe, which was under the assumed water level, and from the upper part of the pipe out of the water level, prove the presence of Zn corrosion products. This was also confirmed by XRD analyses, where zincite,

hydrozincite and wulfingite were identified as the main phases. The presence of calcite from hard water was detected in a small amount.

Using optical microscopy, it was possible to identify the underlying steel as a ferritic-pearlitic structure with a low carbon content. This identification was made outside of the damage area. It was also possible to identify the weld of the pipe, which was located in about the position 3.5-4 o´clock (on the right side of the large tubercules). No damage was observed in the weld area on the galvanizing surface.

By comparing the microstructure of the zinc coating for individual samples, it is possible to assess that the zinc coating on the external part of the pipe is preserved, almost all of them also have pure η-phase – Zn. For the sample that was located out of the presumed water level (top), no big differences in the thickness of the layers (approx. 115 μm) is observed.

The internal layers of the pipeline are significantly damaged, especially for the lower part of the pipeline, where the water level was located. Here, the zinc layer is only about 65 μm thick for one type of sample with a tubercule. For a sample with a tubercule under epoxy, it is approximately 100 μm.

Optical microscopy also shows that the tubercule area significantly damages the zinc layer. This corrosion attack also penetrates the pipe wall itself, weakening it and, in extreme cases, can lead to perforation through the pipe.

From the photo documentation and the analyses, the main problem was the residual water in the cell pipeline and the created cell with different aeration.

Resistometric measurements served to investigate the influence of different aeration on acceleration of corrosion of galvanised steel. According to the results, it can be stated that the zinc surface, especially with good oxygen access, does not contribute to the acceleration of steel corrosion in any combination of macrocells. However, we are at the beginning of the exhibition, and the time factor can of course show itself. The corrosion rates of zinc are very high and over time the surface will be covered with insoluble corrosion products. Zinc corrosion will obviously be faster on the surface immersed in the electrolyte, and the corrosion rate will obviously be higher with a higher oxidizing capacity of the environment. After the steel surface, cells with different aeration begin to appear, but not between Zn and Fe, but between two Fe surfaces - one with worse and the other with better access for oxygen - i.e., steel surface partially covered by corrosion products. The resistometric measurements using electrical resistance probes for revealing the impact of different aeration cell for galvanised steel corrosion will be used in future for long-term exposures.

CONCLUSION

The cause of the pipe damage on the fire protection pipe system was the residual water in the pipe. Due to the pressurised oxygen in the pipe above the water level, places with different aeration are created, which leads to the formation of a cell with differential aeration. This phenomenon is largely responsible for the corrosion attack and for the acceleration of the growth of tubercules on the internal confirmation of the pipeline. The zinc coating in several places of the pipeline no longer fulfils the protective function. The presence of a weld with poor galvanizing quality also contributed to this damage.

The proposed solution in this case would be to slope the pipes so that better drainage of water is ensured during pressure tests and that an aggressive corrosion environment does not arise (cell with differential aeration). The air/oxygen injected into the pipe should be as dry as possible. The second but more costly alternative is pressurizing the pipeline with nitrogen. The last type of solution is the use of a different type of pipe material.

REFERENCES

1. Bednar L. Plain galvanised steel drainage pipe durability estimation with a modified california chart. *Transportation research record* **1989,** 1231: p. 70-78.
2. Su P., Fuller D.B. Corrosion and corrosion mitigation in fire protecting systems. **2014**, p. 98.
3. Piri B. et al. Investigation of failure mechanisms and remaining life prediction of firewater pipelines used in industrial applications. *Engineering Failure Analysis,* **2021**. 124: p. 1-19. https://doi.org/10.1016/j.engfailanal.2021.105301
4. Bravo P.M. et al. Failure analysis of galvanized iron pipeline accessories of a fire protection system. *Engineering Failure Analysis,* **2009**. 16: p. 669-674. https://doi.org/10.1016/j.engfailanal.2008.02.009
5. NFPA 13 Standard for the Installation of Sprinkler Systems. **2022**
6. https://blog.qrfs.com/223-fire-sprinkler-system-pipe-material-nfpa-requirements-and-the-pros-and-cons-of-steel/#:~:text=With%20a%20melting%20point%20that,for%20all%20fire%20protection%20systems. [online,20.3.2023]
7. https://www.chemicalsupport.co.uk/materials/pvc/ [online 28.11.2023].
8. Notarianni K.A., Jackson M.A. Comparison of fire sprinkler piping materials. Building and fire research laboratory. National Institute of Standards and Technology. Gaithersburg. **1994**
9. Chovancová M. et al. Základy korózie a povrchovej úpravy materiálov. Slovenská technická univerzita v Bratislave, Fakulta chemickej a potravinárskej technológie. **2010**, p. 305. ISBN 978-80-227-3378-6
10. Schweitzer P.A. Fundamentals of Corrosion: Mechanisms, Causes, and Preventative Methods. **2010**, p. 430. ISBN 978-1-4200-6770-5

11. Bahrami, A. et al. Establishing the root cause of a failure in a firewater pipeline, *Engineering Failure Analysis*, **2021,** 127: p. 1-10, https://doi.org/10.1016/j.engfailanal.2021.105474.
12. Subramanian CH. Localized pitting corrosion of API 5L grade A pipe used in industrial fire water piping applications. *Engineering Failure Analysis,* **2018**. 92: p. 405-417. https://doi.org/10.1016/j.engfailanal.2018.06.008
13. Andrianov A. Pitting corrosion of galvanised pipes in hot water supply systems. **2021**, https://doi.org/10.1051/e3sconf/202126304035.
14. https://www.ecscorrosion.com/blog/weld-seam-corrosion-causes-and-management [online,28.4.2023].
15. Hopkins M. Avoiding corrosion in dry pipe and preaction sprinkler systems. *Plumbing systems and design.* **2006**. p.34-37.
16. Reiser M. et al. Corrosive synergic effects of acetic acid and atmospheric pollutants on lead and zinc. *KOM – Corrosion and Material Protection Journal,* **2022,** 66: p. 113-125. https://doi.org/10.2478/kom-2022-0015
17. Prosek T. et al. Application of automated electrical resistance sensors for measurement of corrosion rate of copper, bronze and iron in model indoor atmospheres containingshort-chain volatile carboxylic acids. *Corrosion Science*, **2014**. 87: p. 376-382. https://doi.org/10.1016/j.corsci.2014.06.047
18. Vojtěch D. Kovové materiály 1. vyd. Vysoká škola chemicko-technologická v Praze, Praha. **2006,** p.94-96. ISBN-80-7080-600-1.